Study of various resonances within the phonon damping model

Nguyen Dinh Dang

RI-beam factory project office, RIKEN,
2-1 Hirosawa, Wako, 351-0198 Saitama - Japan
and Institute for Nuclear Science and Technique,
Vietnam Atomic Energy Commission - Hanoi, Vietnam
E-mail: dang@rikaxp.riken.go.jp

Abstract. The main successes of the phonon damping model (PDM) are presented in the description of the damping of: 1) The giant dipole resonance (GDR) in highly excited nuclei, 2) The double giant dipole resonance (DGDR) and multiple phonon resonances, 3) The Gamow-Teller resonance (GTR), 4) The damping of pygmy dipole resonance (PDR) in neutron-rich nuclei. The analyses of the results of numerical calculations within the PDM will be discussed in comparison with the experimental systematics on i) the width and the shape of the GDR at finite temperature and angular momentum for tin isotopes, ii) the electromagnetic cross sections for ^{136}Xe and ^{208}Pb on a lead target at relativistic energies, iii) the strength function of GTR, and iv) the PDR in oxygen isotopes.

INTRODUCTION

Although giant resonance is a subject of more than 50 years old, it continues to amaze us with new surprises. Those are the studies of GDR in hot nuclei, the observation of the multiple-phonon giant resonance, the extraction of the high-lying tail of Gamow-Teller resonance (GTR), which recovers the missing part of the Ikeda sum rule, and the measurements of pygmy dipole resonance (PDR) in neutron-rich nuclei. In this talk I will show you how the features of these resonances, especially the PDR and GDR, can be well described within a simple approach called the phonon damping model (PDM), which has been proposed in 1998 by Akito Arima and myself [1].

QUASIPARTICLE REPRESENTATION OF THE PDM

The quasiparticle representation of the PDM Hamiltonian [1,2] is obtained by adding the superfluid pairing interaction and expressing the particle (p) and hole (h) creation and destruction operators, $a_s^\dagger$ and a_s ($s = p, h$), in terms of the quasiparticle operators, $\alpha_s^\dagger$ and α_s, using the Bogolyubov's canonical transformation. The equation for the propagation of the GDR phonon, which is damped due to coupling to quasiparticle field, is given below making use of the double-time Green's function method. The final equation of the Green function for the one-phonon propagation

has the form [3]

$$G_{\lambda i}(E) = \frac{1}{2\pi}\frac{1}{E - \omega_{\lambda i} - P_{\lambda i}(E)} \ , \tag{1}$$

where the explicit form of the polarization operator $P_{\lambda i}(E)$ is

$$P_{\lambda i}(E) = \frac{1}{\hat{\lambda}^2}\sum_{jj'}[f^{(\lambda)}_{jj'}]^2\Big[\frac{(u^{(+)}_{jj'})^2(1-n_j-n_{j'})(\epsilon_j+\epsilon_{j'})}{E^2-(\epsilon_j+\epsilon_{j'})^2}$$

$$-\frac{(v^{(-)}_{jj'})^2(n_j-n_{j'})(\epsilon_j-\epsilon_{j'})}{E^2-(\epsilon_j-\epsilon_{j'})^2}\Big]. \tag{2}$$

The presence of polarization operator (2) due to ph – phonon coupling in the PDM Hamiltonian, and the analytic property of the double-time Green's function allows the damping to be calculated in an explicit and microscopic way. Namely, the phonon damping $\gamma_{\lambda i}(\omega)$ (ω real) is obtained as the imaginary part of the analytic continuation of the polarization operator $P_{\lambda i}(E)$ into the complex energy plane $E = \omega \pm i\varepsilon$:

$$\gamma_{\lambda i}(\omega) = \frac{\pi}{2\hat{\lambda}^2}\sum_{jj'}[f^{(\lambda)}_{jj'}]^2\Big\{(u^{(+)}_{jj'})^2(1-n_j-n_{j'})[\delta(E-\epsilon_j-\epsilon_{j'})-\delta(E+\epsilon_j+\epsilon_{j'})]-$$

$$(v^{(-)}_{jj'})^2(n_j-n_{j'})[\delta(E-\epsilon_j+\epsilon_{j'})-\delta(E+\epsilon_j-\epsilon_{j'})]\Big\}. \tag{3}$$

The energy $\bar{\omega}$ of giant resonance (damped collective phonon) is found as the pole of the Green's function (1):

$$\bar{\omega} - \omega_{\lambda i} - P_{\lambda i}(\bar{\omega}) = 0 \ . \tag{4}$$

The width Γ_λ of giant resonance is calculated as twice of the damping $\gamma_\lambda(\omega)$ at $\omega = \bar{\omega}$, i.e.

$$\Gamma_\lambda = 2\gamma_\lambda(\bar{\omega}), \tag{5}$$

where $\lambda = 1$ corresponds to the GDR. The line shape of the GDR is described by the strength function $S_{\rm GDR}(\omega)$, which is derived from the spectral intensity in the standard way using the analytic continuation of the Green function (1) and by expanding the polarization operator (2) around $\bar{\omega}$:

$$S_{\rm GDR}(\omega) = \frac{1}{\pi}\frac{\gamma_{\rm GDR}(\omega)}{(\omega-\bar{\omega})^2+\gamma^2_{\rm GDR}(\omega)} \ . \tag{6}$$

The photoabsorption cross section $\sigma(E_\gamma)$ is calculated from the strength function $S_{\rm GDR}(E_\gamma)$ as

$$\sigma(E_\gamma) = c_1 S_{\rm GDR}(E_\gamma)E_\gamma \ , \tag{7}$$

where $E_\gamma \equiv \omega$ is used to denote the energy of γ-emission. The normalization factor c_1 is defined so that the total integrated photoabsorption cross section $\sigma = \int \sigma(E_\gamma) dE_\gamma$ satisfies the GDR sum rule $\mathrm{SR_{GDR}}$, hence

$$c_1 = \mathrm{SR_{GDR}} \Big/ \int_0^{E_{\max}} S_{\mathrm{GDR}}(E_\gamma) E_\gamma dE_\gamma \ . \tag{8}$$

In heavy nuclei with $A \geq 40$, the GDR exhausts the Thomas-Reich-Kuhn (TRK) sum rule $\mathrm{SR_{GDR}} = \mathrm{TRK} \equiv 60\ NZ/A$ (MeV·mb) at the upper integration limit $E_{\max} \simeq 30$ MeV, and exceeds TRK ($\mathrm{SR_{GDR}} > \mathrm{TRK}$) at $E_{\max} > 30$ MeV due to the contribution of exchange forces. In some light nuclei, such as ^{16}O, the observed photoabsorption cross section exhausts only around 60% of TRK up to $E_{\max} \simeq 30$ MeV [4]. The EM cross section σ_{EM} is calculated from the corresponding photoabsorption cross section $\sigma(E_\gamma)$ and the photon spectral function $N(E_\gamma)$ according to [5,6]. In the numerical results discussed below the GTR and PDR have been calculated including pairing. The results for the hot GDR and DGDR are presented neglecting pairing.

GDR IN HIGHLY EXCITED NUCLEI AND MULTIPLE PHONON GDR

The PDM has been proved to be quite successful in the description of the width and the shape of the GDR as a function of temperature T [1,2,7] and angular momentum J [8]. An example is shown in Fig. 1. The PDM has resolved the long-standing

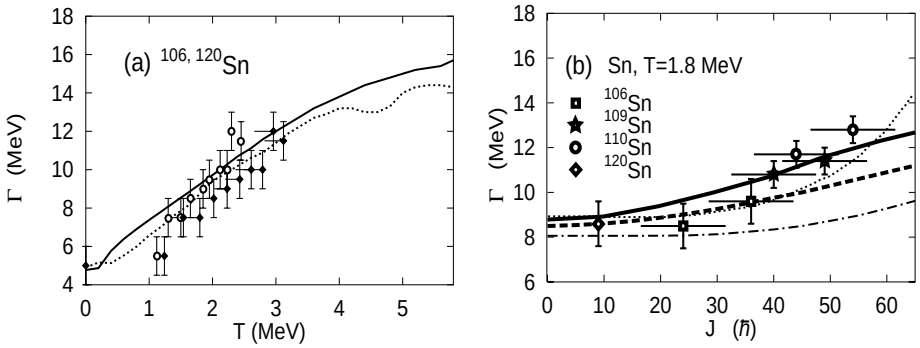

Figure 1: GDR width as a function of temperature T (a) and angular momentum J (b) in tin isotopes. In (a) the solid line is the width for ^{106}Sn, while the one for ^{120}Sn is given by the dotted line. In (b) the thick solid and dashed lines are results obtained within PDM for ^{106}Sn and ^{120}Sn, respectively, while the corresponding results within the thermal fluctuation model are given by dotted and dash-dotted lines, respectively. The data points in (a) and (b) are taken from [9] and [10], respectively.

problem with the electromagnetic (EM) cross sections of the DGDR in ^{136}Xe and

^{208}Pb, in which the prediction by the non-interacting phonon picture underestimated significantly the observed DGDR cross sections by the LAND collaboration. The prediction using the strength functions obtained within PDM [11] is given in Fig. 2 in comparison with the latest results of data analyses by LAND collaboration [12]. The agreement between the PDM prediction and the data is remarkable. The PDM also predicted the DGDR at non-zero temperature [13], which has been confirmed experimentally in a very recent work by Viesti et al [14].

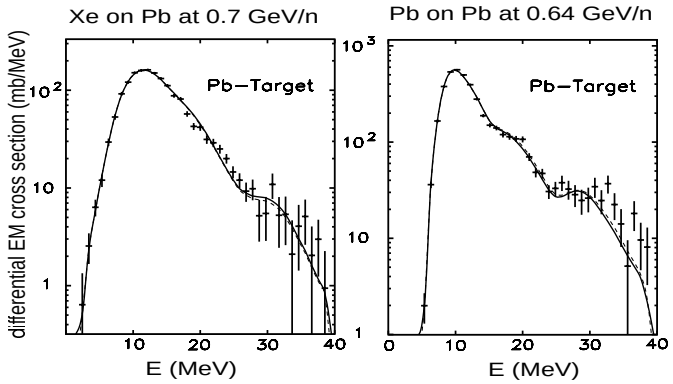

Figure 2: EM cross sections of GDR and DGDR for ^{136}Xe and ^{208}Pb. The solid lines are theoretical predictions, in which the DGDR strength functions within PDM are used. The data points are results of the LAND collaboration [12]. The dashed lines show the best fit using χ^2. The theoretical results have been folded with the detector response by K. Boretzky [12].

GAMOW-TELLER RESONANCE

Shown in Fig. 3 is the prediction of [15] within the PDM-1 [1] (solid line), and PDM-2 [2] (dashed line) for the GTR in ^{90}Nb in comparison with the result obtained within a microscopic theory which explicitly includes coupling to $2p2h$ configurations in terms of two-phonon configurations (dotted line) [16], and the experimental data (data points with errorbars) [17]. Again, the agreement between theory and experiment is quite reasonable.

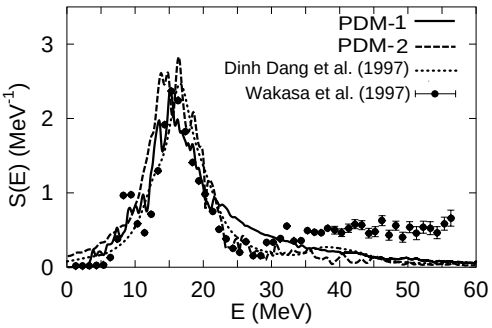

Figure 3: Strength functions of the GTR in 90Nb. See text for the notation.

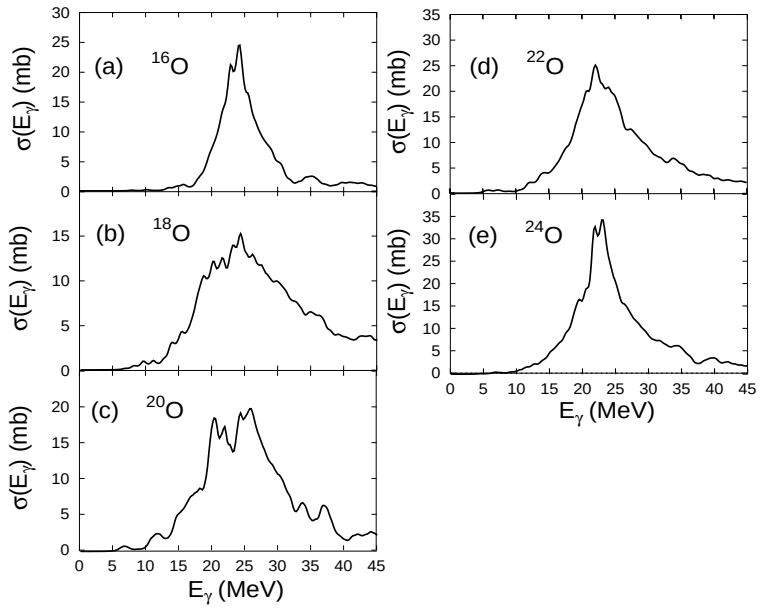

Figure 4: Photoabsorption cross sections for oxygen isotopes obtained within PDM.

Shown in Fig. 4 are the photoabsorption cross sections $\sigma(E_\gamma)$, which have been obtained within PDM for oxygen isotopes. The shapes of the photoabsorption cross section calculated for stable isotopes ^{16,18}O and ^{40,48}Ca are found in overall reasonable agreement with available experimental data as shown in the left panels of Fig. 5 ((a) - (d)). This agreement is better than those given by several other models shown in the right panels of Fig. 5 ((e) - (h)), namely the large-scale shell model (LSSM) [18] (thin solid and thin dashed lines in (e) and (f) with $T_< = 1$ and $T_> = 2$ denoting two isospin components of GDR in ^{18}O), the surface coupling model (SCM) [19] (dotted lines in (e) and (g)), the second RPA (SRPA) [20] (thick dashed line in (g)), and a microscopic model including $1p1h\otimes$phonon plus continuum (phPC) [21] (dash-dotted lines in (g) and (h)). It is seen from Fig. 4 that the GDR becomes broader for isotopes with $N > Z$. Its width is particularly large for isotopes between the double closed shell ones, such as ^{18,20}O. The increase of GDR spreading enhances both of its low- and high-energy tails. In the region $E_\gamma \leq 15$ MeV, some weak structure of PDR is visible for ^{18,20,22}O. In the rest of isotopes under study, except for an extension of the GDR tail toward lower-energy, there is no visible structure of PDR.

The fractions of the EWS of strength exhausted by the low-energy tail of GDR are shown in Figs. 6. The trend obtained within PDM for oxygen isotopes reproduces the one observed in the recent experiments at GSI [22], which shows a clear deviation from the prediction by the cluster sum rule (CSR). The agreement

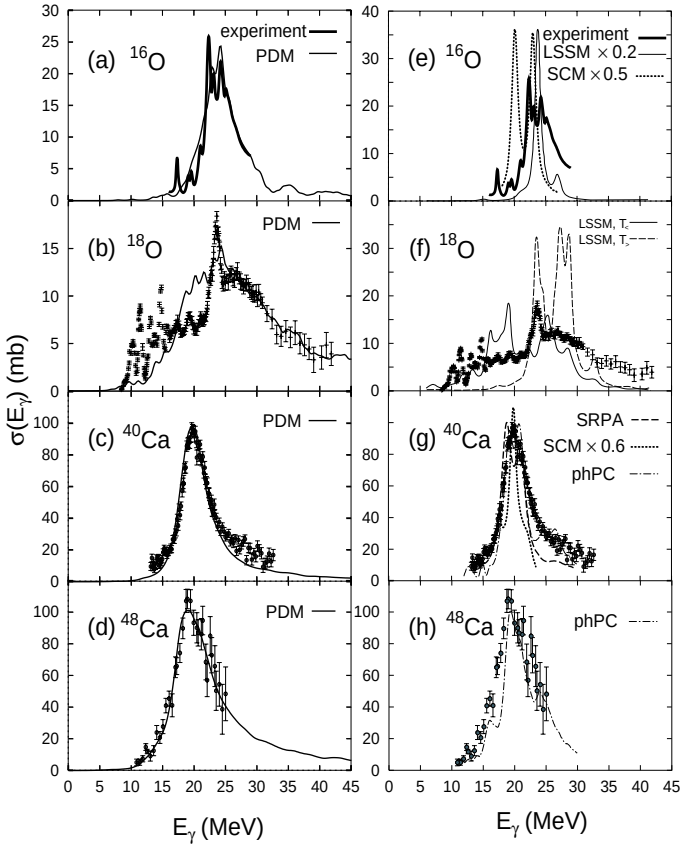

Figure 5: Photoabsorption cross sections for ^{16,18}O and ^{40,48}Ca obtained within PDM (left panels) and within other models mentioned in the text (right panels) in comparison with experimental data for ^{16}O (thick solid line in (a) and (e)), ^{18}O ((b) and (f)), ^{40}Ca ((c) and (g)), and ^{48}Ca ((d) and (h)).

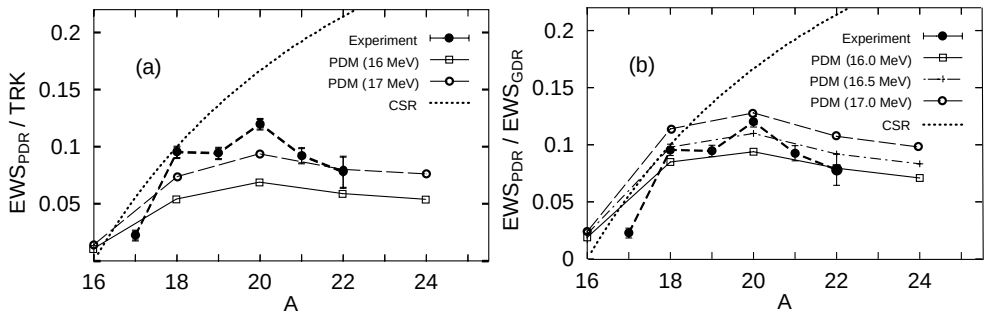

Figure 6: EWS of PDR strength up to excitation energy $E_{\max}$ for oxygen isotopes. Results obtained within PDM with $E_{\max} = 16$, 16.5, and 17 MeV are displayed as open boxes connected with solid line, crosses connected with dash-dotted line, and open circles connected with thin dashed line, respectively. In (a) the PDM results are shown in units of TRK, while in (b) they are in units of the total GDR strength integrated up to 30 MeV. Experimental data (in units of TRK), obtained with $E_{\max} = 15$ MeV, are shown by full circles connected with thick dashed line. The dotted line is the prediction by the cluster sum rule (CSR) (in units of TRK).

between the PDM prediction and the experimental data for the photoabsorption cross sections as well as for the EWS of PDR strength suggests that the mechanism of the damping of PDR is dictated by the coupling between the GDR phonon and noncollective *ph* excitations rather than by the oscillation of a collective neutron excess against the core. Strong pairing correlations also prevent the weakly bound neutrons to be decoupled from the rest of the system [23]. Only when the GDR is very collective so that it can be well separated from the neutron excess, the picture of PDR damping becomes closer to the prediction by the CM. The photon

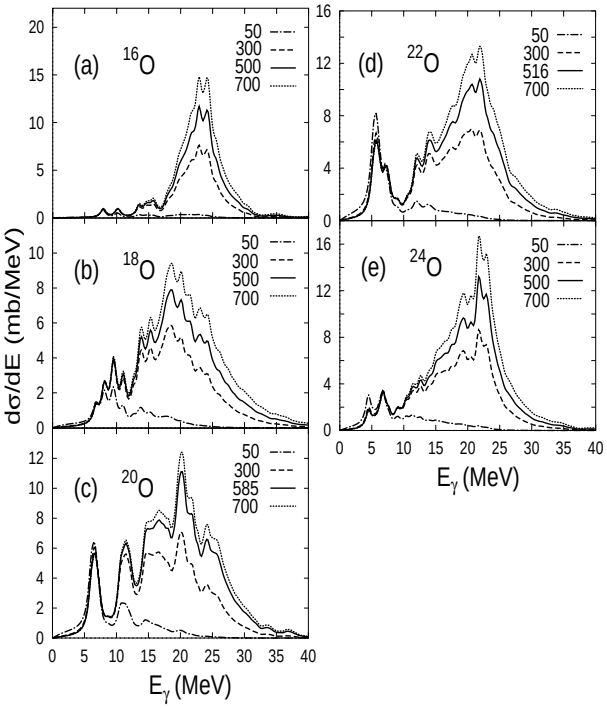

Figure 7: Electromagnetic cross sections of E1-excitations within PDM for oxygen isotopes on ^{208}Pb target. Different lines display results obtained at different projectile energies, whose values (in MeV/nucleon) are indicated in the panels.

spectral function $N(E_\gamma)$ in the EM differential cross section $d\sigma_{\rm EM}/dE_\gamma$ contains an exponentially decreasing factor $e^{-m(b)}$ with increasing E_γ. This behavior enhances the low-energy part of the E1 strength in the EM differential cross section. These EM differential cross sections obtained within PDM are shown in Fig. 7 for oxygen isotopes. The PDR shows up in the EM cross sections of all neutron-rich isotopes, especially for ^{20,22}O, where a well isolated peak located at around 7 MeV is clearly seen. The PDR becomes depleted when the neutron number approaches a magic number (where the GDR is most collective) as can be seen in calcium isotopes when N increases from 20 to 28. Therefore, the decrease of PDR strength in ^{24}O can be understood as the depletion on the way toward the next magic number $N = 28$. Because of the behavior of $N(E_\gamma)$, the decrease of the projectile energy from

700 MeV/nucleon to 300 MeV/nucleon strongly reduces the EM cross section in the GDR region (above 10 MeV), but leaves the PDR almost intact, as can be seen in Fig. 7. A further decrease of projectile energy to 50 MeV/nucleon suppresses completely the GDR peak and even enhances the PDR peak in some very neutron-rich nuclei ^{20,22,24}O (dash-dotted lines in Fig. 7). This observation shows that, using high-intensity RI beams at low energies of around 50 – 60 MeV/nucleon, one may be able to observe a rather clean and sharp PDR peak in ^{20,22}O in the region around 7 MeV.

CONCLUSIONS

The PDM is a simple yet microscopic model, which can describe rather well various resonances and has resolve several long standing problems including the width and shape of the hot GDR, the electromagnetic cross section of the DGDR, the quenching of the GTR. It also predicts the PDR in neutron-rich nuclei and the DGDR in hot nuclei.

REFERENCES

1. N. Dinh Dang and A. Arima, Phys. Rev. Lett. **80** (1998) 4145, Nucl. Phys. **A 636** (1998) 427.
2. N. Dinh Dang. K. Tanabe, and A. Arima, Phys. Rev. **C 58** (1998) 3374, Nucl. Phys. **A 645** (1999) 536.
3. N. Dinh Dang, V. Kim Au, T. Suzuki, and A. Arima, Phys. Rev. **C 63** (2001) 44302.
4. J.G. Woodworth et al., Phys. Rev. **C 19** (1979) 1667.
5. W. J. Llope and P. Braun-Muzinger, Phys. Rev. C **41**, (1990) 2644.
6. I.A. Pshenichnov *et al.*, Phys. Rev. C **60** (1999) 044901.
7. N. Dinh Dang, K. Eisenman, J. Seitz, and M. Thoennessen, Phys. Rev. **C 61** (2000) 027302
8. N. Dinh Dang, Nucl. Phys. **A 687** (2001) 253c.
9. T. Baumann et al., Nucl. Phys. **A 635** (1998) 428, **A649** (1999) 173c.
10. A. Bracco et al., Phys. Rev. Lett. **74** (1995) 3748, M. Matiuzzi et al., Nucl. Phys. **A 612** (1997) 262.
11. N. Dinh Dang, V. Kim Au, and A. Arima, Phys. Rev. Lett. **85** (2000) 1827.
12. K. Boretzky, private communication (September, 2000).
13. N. Dinh Dang, K. Tanabe, and A. Arima, Phys. Rev. **C 59** (1999) 3128.
14. G. Viesti et al., Phys. Rev. **C 63** (2001) 034611.
15. N. Dinh Dang. T. Suzuki. and A. Arima, Phys. Rev. **C 64** (2001) 27303.
16. N. Dinh Dang et al., Nucl. Phys. **A 621** (1997) 719.
17. T. Wakasa et al., Phys. Rev. **C 55** (1997) 2909.
18. H. Sagawa and T. Suzuki, Phys. Rev. **C 59** (1999) 3116.
19. P.F. Bortignon and R.A. Broglia, Nucl. Phys. **A 371** (1981) 405.
20. S. Nishizaki and J. Wambach, Phys. Lett. **B 349** (1995) 7.
21. S. Kamerdzhiev, J. Speth, and G. Tertychny, Nucl. Phys. **A 624** (1997) 328.
22. T. Aumann et al., GSI Scientific Report 1999 (2000) 27.
23. S. Mizutori et al., Phys. Rev. **C 61** (2000) 044326.